ACS Catalysis

Research Article

pubs.acs.org/acscatalysis

Influence of ZnO Facets on Pd/ZnO Catalysts for Methanol Steam Reforming

He Zhang,[†] Junming Sun,[†] Vanessa L. Dagle,[‡] Barr Halevi,[§] Abhaya K. Datye,[§] and Yong Wang*[,†,‡]

[†]The Gene & Linda Voiland School of Chemical Engineering and Bioengineering, Washington State University, Pullman, Washington 99164, United States

[‡]Institute for Integrated Catalysis, Pacific Northwest National Laboratory, Richland, Washington 99352, United States

[§]Department of Chemical & Nuclear Engineering and Center for Microengineered Materials, MSC01 1120, University of New Mexico, Albuquerque, New Mexico 87131, United States

Supporting Information

ABSTRACT: A series of Pd/ZnO catalysts with different Pd loadings were prepared using needlelike ZnO crystallites (ZnO-N) with predominant (10−10) nonpolar facets exposed and commercial ZnO (ZnO-P) without any dominant facets. The Pd/ZnO catalysts were characterized using complementary techniques, such as nitrogen physisorption, X-ray diffraction (XRD), high-resolution transmission electron microscopy (HRTEM), and Fourier transform infrared spectroscopy analysis of adsorbed CO (CO-FTIR). The effect of ZnO crystallite faceting on the activity and selectivity of the Pd/ZnO catalysts was studied in methanol steam reforming (MSR). It was found that the Pd-rich phases (Pd_xZn_y, $x > y$) are predominantly formed at low Pd loadings on both ZnO supports (ZnO-N and ZnO-P), resulting in high CO selectivity. As Pd loading increases, the x/y ratio in the Pd_xZn_y phases decreases, leading to decreased CO selectivity. At similar Pd loadings, Pd/ZnO-P catalysts are more selective in MSR than Pd/ZnO-N, which is due to more facile formation of the stable $PdZn_\beta$ phase on polar ZnO (0001) facets than on nonpolar ZnO (10−10) facets. The current study provides insight into the structure−performance relationships in Pd/ZnO catalysts for MSR, helping shed light on the rational design of selective MSR catalysts to minimize CO formation.

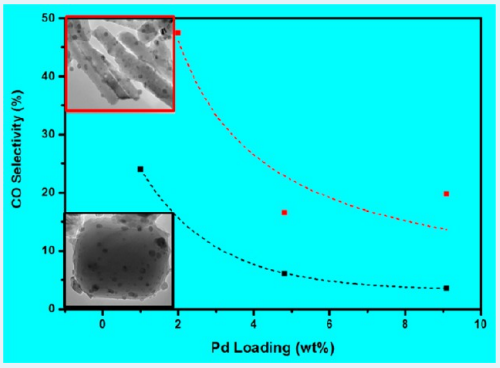

KEYWORDS: *ZnO facet, PdZn alloy, $PdZn_\beta$, Pd-rich, metallic Pd, methanol steam reforming, MSR, CO selectivity*

1. INTRODUCTION

Methanol steam reforming (MSR) has been extensively studied for hydrogen production,[1−4] primarily because of the high hydrogen/carbon ratio, low sulfur content, and relatively low reforming temperature (200−300 °C) of methanol. In their pioneering work, Iwasa et al.[5] showed that the Pd/ZnO catalyst is highly active and selective for MSR. The high selectivity to CO_2 (low CO selectivity) was attributed to the formation of PdZn alloy (Pd/Zn = 1:1) via reduction of Pd/ZnO in H_2 at >350 °C. Subsequently, the effects of the PdZn particle size and the extent of PdZn alloy formation were investigated.[6−8] Large PdZn alloy particles were found to be essential to minimize the CO formation in MSR. Even for Pd/ZnO catalysts with low extent of bulk PdZn alloy formation, surface PdZn alloy was found to exhibit low CO selectivity in MSR, which was attributed to a much lower methanol decomposition rate than that for steam reforming.[7] In addition, catalyst support was also found to affect catalytic activity and CO selectivity.[4,9−11] Recent studies on aerosol-derived $PdZn_\beta$ and $PdZn_\alpha$ particles suggest that CO selectivity in MSR is low on the $PdZn_\beta$ phase having Pd/Zn = 1:1, whereas $PdZn_\alpha$, which is Pd-rich with Pd/Zn = 5.7:1, favors CO formation during MSR.[12−14] More recent studies[15] on unsupported intermetallic PdZn catalysts have revealed that Pd-rich Pd_xZn_y ($x > y$) catalysts exhibit limited activity and very high selectivity to CO in MSR, whereas Zn-rich Pd_xZn_y ($y > x$) catalysts have good activity and low CO selectivity (as low as 0.6%).

ZnO has been found to serve several roles in Pd/ZnO catalysts for MSR, and it was initially used as the active component to form the PdZn alloy.[5] The role of water activation on ZnO has been proposed to be essential to the high activity and selectivity to CO_2 in the Pd−Zn catalyst system.[15,16] The combination of high-surface-area PdZn for methanol adsorption and ZnO islands for water activation led to facile methanol steam reforming toward H_2 and CO_2.[16] However, it is unclear why a high CO selectivity was achieved on highly dispersed PdZn on ZnO (e.g., 0.5 wt % Pd/ZnO reduced at temperatures higher than 350 °C[6]), on which close interaction between the small PdZn bimetallic particles and ZnO support could also be expected. On the other hand, the

Received: March 24, 2014
Revised: May 29, 2014
Published: June 6, 2014

   dx.doi.org/10.1021/cs500590t | ACS Catal. 2014, 4, 2379−2386

ZnO facet of Pd/ZnO catalyst was found to play an important role in MSR. For example, it was found that, compared with acidic precursor (e.g., Pd nitrate in nitric acid), mild ones (i.e., Pd acetate in acetone) preserved faceted ZnO and led to higher MSR activity.[7]

It is well-known that polar facets of the oxide influence the formation of a stable metal/oxide interface. ZnO is a direct wide-band-gap semiconductor and has been widely used in optical, electronic and catalytic fields. A ZnO crystal consists of a positively charged plane (0001) terminated with zinc, a negatively charged plane (000-1) terminated with oxygen, and nonpolar planes, mainly including the (10-10). The polar (0001) facet of ZnO has been found to be unstable, and surface energy can diverge to infinity as a result of residual dipole moments. Depending on the polarity, the terminating atomic species and the interfacial charge can be manipulated, as seen from HRTEM investigations of Pd/ZnO systems.[17]

There have been a few reports regarding the facet effect of bare ZnO on catalytic reactions.[18,19] For example, hexagonal platelike ZnO was shown to exhibit more than 5 times higher activity than rod-shaped particles in the photocatalytic decomposition of methylene blue.[18] As far as we know, there is still no report of a ZnO facet effect on MSR for high-surface-area Pd/ZnO catalysts. However, ultrahigh vacuum (UHV) single crystal studies have shown that ZnO facets affect CO and methanol desorption in the Pd/ZnO model catalyst system, and the formation of a PdZn alloy is potentially easier on the (0001) polar facets of ZnO.[20] This triggered our interest in the fundamental understanding of the effect of ZnO facets on the surface composition and performance of high surface area Pd/ZnO catalyst for MSR.

Previous studies of facet influence on catalytic reactions were exclusively conducted using single-crystal model surfaces in an UHV system.[21−24] Compared with the practical high surface area catalysts that are used under ambient or elevated pressures, there are material and pressure gaps between UHV and practical catalyst systems. Recent advances in materials science provide the potential to prepare metal and metal oxide crystals with dominantly exposed planes that can be used to close the material and pressure gap with the UHV studies. There have been some reports in specific metal or metal oxide catalytic reactions. Among these, the facet effects of Pt,[25] Ag,[26] Co_3O_4,[27] ZnO,[18,28] CeO_2,[29] etc. have been investigated in certain catalytic or photocatalytic reactions. However, there are rare studies on the ZnO facet effect of Pd/ZnO catalysts in MSR. To study the effects of the ZnO facet in high-surface-area catalysis, it is highly desirable to synthesize ZnO with different dominantly exposed facets that are stable at elevated temperatures for both the MSR reaction (>200 °C) and catalyst reduction (>350 °C).

There are some strategies available to prepare highly preferred faceted ZnO, such as the oleic acid (OA) microemulsion solvent thermal process.[18,30−32] However, the obtained ZnO are only several nanometers (<10 nm) in certain dimensions, which can readily aggregate under a high temperature pretreatment.[33] The polyvinylpyrrolidone (PVP)-assisted alcohol thermal procedure is a facile route to obtain different morphological ZnO, such as rods, hexagonal plates, prisms, and spheres, and some of them have a few dominant planes.[32,34] The particle size of the synthesized materials is relatively larger than those obtained by OA microemulsion method; therefore, it is relatively easier to preserve their dominant facets at high temperature. Herein, we used alcohol thermal process to synthesize stable ZnO needle (ZnO-N) with dominant (10−10) nonpolar facets. The influence of ZnO facets on the structure of Pd_xZn_y alloy and the catalytic performances in MSR was investigated over Pd/ZnO-N catalysts in comparison with the commercial ZnO prism (ZnO-P) without any dominant facets.

2. MATERIALS AND METHODS

2.1. Catalysts Preparation. Two series of Pd/ZnO catalysts were prepared using a commercial ZnO prism (ZnO-P, Sigma-Aldrich, >99%) without dominant facets and a needlelike ZnO (ZnO-N) with predominantly exposed nonpolar facets, that is, (10-10). The ZnO needles were synthesized using a PVP assisted alcohol thermal procedure according to a previously reported method[34] with some modifications. In a typical synthesis, 3 g of PVP (Sigma-Aldrich; M = 40 000) was dissolved in 180 mL of ethanol (200 proof), and then 0.75 g of zinc acetate dihydrate (Sigma-Aldrich, reagent grade) was slowly added into the solution. The resulting mixture was stirred for several minutes, followed by addition of 4.5 g of NaOH. A turbid solution resulted and was stirred for another 2 h. The above solution was loaded and sealed into an autoclave, which was kept at 80 °C for 24 h. Then, the sample was filtered and washed with ethanol and distilled water several times. Finally, the precipitate was dried to obtain the as-synthesized ZnO-N. PVP could be still observed surrounding some of the particles by TEM, even after repeated ethanol and water washes (Supporting Information Figure S1). However, PVP could be removed completely after calcination at 350 °C for 3 h.

To prevent the ZnO surface structure[6] from being affected by chemically active precursors such as nitrates, the catalysts were prepared by impregnating the ZnO support with palladium II acetate salt (>99.9%, Sigma-Aldrich) dissolved in acetone, followed by drying at 80 °C for 8 h and calcined at 350 °C for 3 h. For each series, the Pd loading amount (wt %) was varied between 1% and 9.1%.

2.2. Catalysts Characterization. ZnO samples and Pd/ZnO catalysts were characterized using XRD, N_2-sorption, TEM/HRTEM, and CO-FTIR. No apparent catalyst deactivation was observed for all the catalysts studied within the 4−5 h of investigated time on stream (TOS). All the spent Pd/ZnO catalysts are characterized by XRD and TEM/HRTEM. For in situ tests of CO-FTIR, pretreatment of catalysts was similar to that used during the MSR reaction.

X-ray diffraction (XRD) spectra were recorded using a Philips X'pert MPD (model PW3040/00) diffractometer with copper anode ($K\alpha_1$ = 0.154 05 nm) and a scanning rate of 0.04° per second at 2θ = 20°−70°. The diffraction patterns were analyzed using Jade 5 (Materials Data Inc., Livermore, CA) and the Powder Diffraction File database (International Center for Diffraction Data, Newtown Square, PA). The particle size of the ZnO crystals was estimated from the XRD patterns using the Scherrer equation ($d = 0.89\lambda/(B \cos \theta)$, where λ is the wavelength of Cu Kα radiation, B is the calibrated full width at half-maximum (fwhm) of the peak in radians, and θ is the diffraction angle of the crystal plan).

Nitrogen sorption experiments were recorded on a Micromeritics TriStar II 3020 Automatic Physisorption Analyzer. Before adsorption analysis, samples were degassed under vacuum at 573 K for 1 h.

Transmission electron microscopy (TEM) was conducted using a JEOL 2010 high-resolution analytical electron micro-

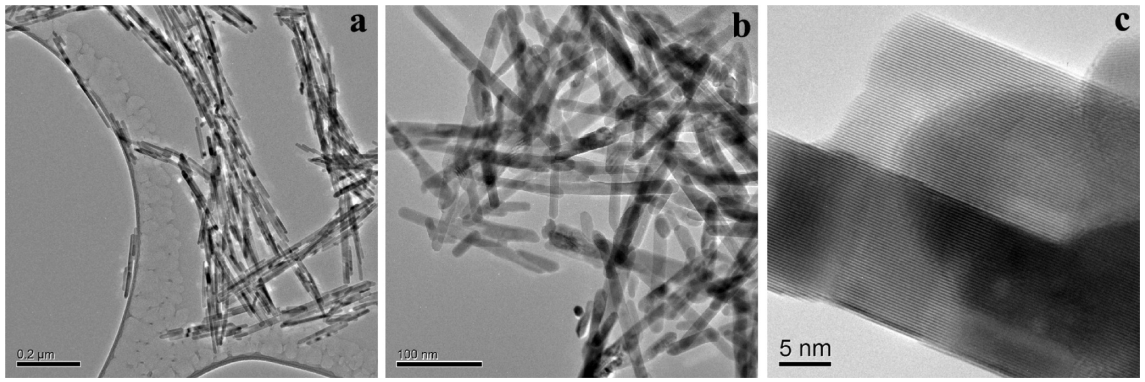

Figure 1. TEM images of ZnO-N (a) as-synthesized and (b, c) calcined.

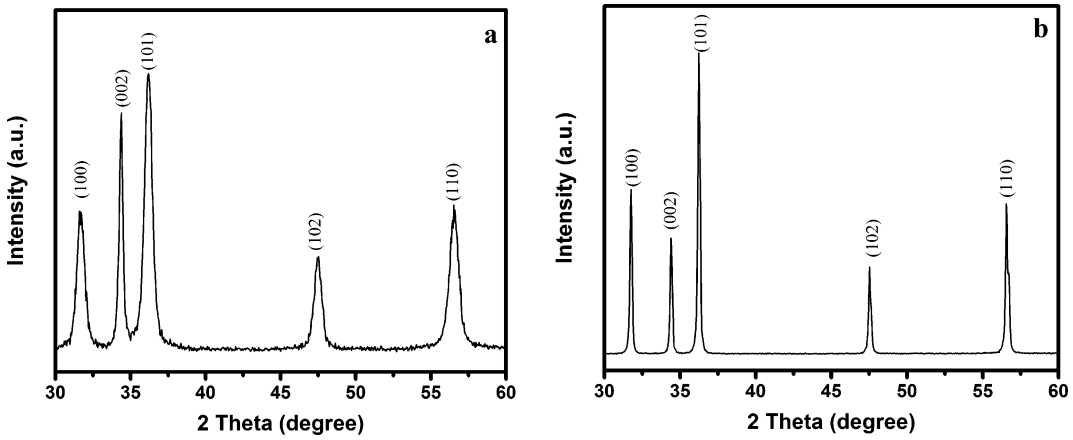

Figure 2. XRD patterns of calcined (a) ZnO-N and (b) ZnO-P.

scope operating at 200 kV with a LaB_6 filament. To determine the average number particle size of Pd or PdZn, we counted a few hundred (300−500) particles in the different images. Scanning and high-resolution transmission electron microscopy (STEM and HRTEM) were performed on a JEOL 2010F FASTEM field emission gun scanning transmission electron microscope equipped with EDS. The probe size of 0.3 nm was used for imaging, and 1.0 nm for analytical work; and accelerating voltage was 200 kV. Pdf's 01-072-2936, 00-046-1043, and 00-036-1451 were used to index $PdZn_{\beta}$, $PdZn_{\alpha}$, and ZnO, respectively.

CO-FTIR was used to probe surface composition of the catalysts by CO adsorption at room temperature, followed by Fourier transform infrared spectroscopy (FTIR).[35] FTIR spectra were recorded with a Bruker spectrometer, equipped with a MCT detector (resolution, 4 cm^{-1}, 128 scans). The samples pressed into a pellet were first pretreated under H_2 for 2 h at the corresponding temperature. During this pretreatment, the sample was alternately exposed to H_2 for 30 min and evacuated under vacuum for 15 min. After that, the temperature was cooled to room temperature, and small doses of CO were progressively added until saturation of the catalyst surface occurred.

2.3. Catalytic Reaction. Methanol steam reforming reactions were evaluated in a 4 mm i.d. quartz tube reactor at 250 °C, described elsewhere.[6] 100 mg of Pd/ZnO-N or 200 mg of Pd/ZnO-P catalysts were loaded between two layers of quartz wool inside the reactor. To achieve intermetallic PdZn with comparable particle size, all the Pd/ZnO-N catalysts and 1% Pd/ZnO-P were reduced in situ under 10% H_2/N_2 at 400 °C for 2 h, and 350 °C was used for the reduction of 4.8% Pd/ZnO-P and 9.1% Pd/ZnO-P. Following the reduction, these catalysts were cooled to 250 °C for catalytic evaluations. A premixture feed of water/methanol (molar ratio of 1.8:1) was pumped into a vaporizer operating at 180 °C and carried into the reactor by flowing N_2. Different flow rates of the liquid feed (0.3−2 mL/h) were used while keeping the methanol/water/N_2 partial pressure constant (6.4 mol% methanol). Reaction products (H_2, CO, CO_2) were analyzed by using an online Micro-GC (MicroGC 3000A) equipped with TCD detectors.

3. RESULTS AND DISCUSSION

3.1. ZnO-N Support with Dominant Nonpolar (10-10) Facets. BET surface areas of the ZnO-N and ZnO-P are 36 and 4 m^2/g, respectively. Figure 1 shows the TEM image for ZnO-N. They have needlelike morphology with 50−200 nm length, 10−20 nm width, and predominant exposure of the (10−10) facets. The XRD patterns for both ZnO samples display the expected ZnO Wurtzite structure as shown in Figure 2. It is noteworthy that the peaks characteristic of (100) and (101) on ZnO-N are clearly broadened (Figure 2a), suggesting nanosized dimensions. According to the Scherrer equation, the average dimensions calculated for ZnO-N are 14.7, 36.4, and 15.7 nm, corresponding to the (100), (002), and (101) planes, which suggests that the particles are elongated along the [0001] direction such that the polar ZnO surfaces are at the tips of the needles. These results are consistent with the TEM observations. In contrast, for the commercial ZnO with dimensions (>100 nm) of the (100), (002), and (101) planes, is demonstrated by TEM that there is no substantial

dx.doi.org/10.1021/cs500590t | ACS Catal. 2014, 4, 2379−2386

preferential facet exposure of either polar or nonpolar surfaces (Supporting Information Figure S2). The ZnO-N sample therefore has a higher proportion of the nonpolar facets than the commercial ZnO-P, and these two supports can therefore be used to prepare ZnO-supported PdZn catalysts and study the effects of ZnO faceting in MSR.

Because the effect of faceting is being studied, it is important to note that the ZnO morphology is maintained at the conditions used, as evident from the following. From XRD of a calcined sample at 350 °C, ZnO needles represent a stable ZnO material and could be applied in some high-temperature catalytic reaction, such as MSR at 250 °C.

3.2. Pd/ZnO Catalysts with Different Pd Loading. Figure 3 shows the XRD patterns of Pd/ZnO-N catalysts with different Pd loading after reduction in H_2 at 400 °C. Diffraction peaks characteristic of ZnO for Pd/ZnO-N are similar to those on the ZnO-N, and the calculated dimensions corresponding to (100), (002), (101) of 9.1% Pd/ZnO-N are still 23.1, 42.6, and 23.6 nm, respectively. Apparently, the dominant nonpolar facets of ZnO needles are maintained even after high-temperature reduction, indicating ZnO-N-supported Pd catalysts are stable for MSR. Over the 2 wt % Pd/ZnO-N, only one broad peak was observed at 41.2°, which can be assigned to the (111) peak of the tetragonal PdZn $L1_0$ intermetallic phase with extremely small particle size.[8,12,14] With the increase in Pd loading, the peak becomes more distinct, and diffraction peaks of PdZn (100) can also be discerned. No obvious metallic Pd was detected by XRD over all three catalysts. The PdZn particle sizes calculated from XRD are ~4 and 16 nm for 4.8 and 9.1 wt % Pd samples. For 2 wt % Pd/ZnO-N, the Pd-related peaks are too broad to calculate the particle size. Similarly, the catalysts prepared with the commercial ZnO support led to formation of the PdZn alloy at 4.8% and 9.1% Pd loadings (Supporting Information Figure S3), with average PdZn crystallite sizes of 28 and 32 nm (measured by XRD), respectively. Only ZnO peaks were evident for the 1 wt % Pd sample because the particle size of 1 wt % Pd loading could be below the measurement threshold for XRD.

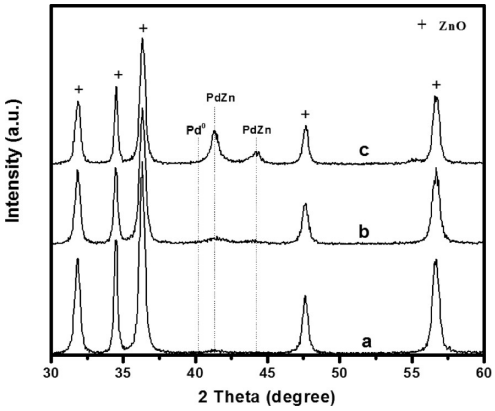

Figure 3. XRD patterns of Pd/ZnO-N with a Pd loading amount of (a) 2%, (b) 4.8%, and (c) 9.1%.

Consistent with the XRD results, TEM images (Figure 4) of the three catalysts confirm that the needlelike morphology and dominant nonpolar facets of ZnO were well preserved after the reduction step, which was used to form the PdZn alloy at high temperature. For the three catalysts, there exists some amount of very small metallic particles (<2 nm); however, with the increase of Pd loading, the fraction of large particles as well as the average particle size increases. Details of the particle sizes and related characterization of the catalysts are summarized in Table 1. The particle size of PdZn on ZnO-P is slightly larger than those on ZnO-N, likely due to the smaller surface area for ZnO-P than that for ZnO-N. In general, XRD-derived average particle sizes are larger than those obtained by TEM because particles smaller than 2 nm are beyond the detection limit of XRD.

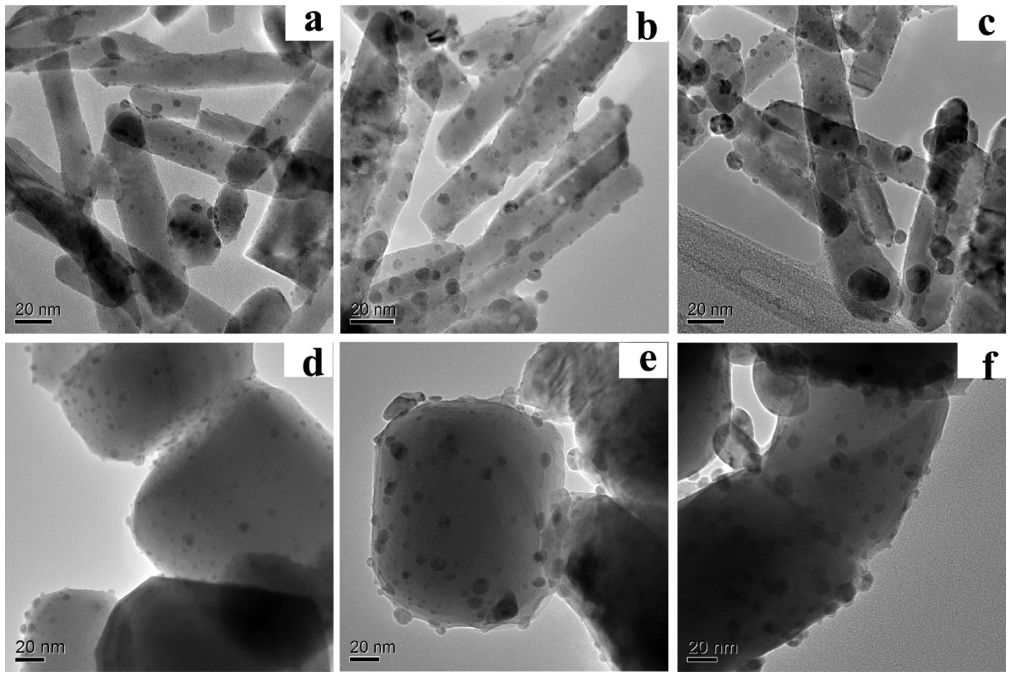

Figure 4. TEM images of Pd/ZnO with different Pd loading amounts. Pd/ZnO-N: (a) 2%, (b) 4.8%, (c) 9.1%. Pd/ZnO-P: (d) 1%, (e) 4.8%, (f) 9.1%.

dx.doi.org/10.1021/cs500590t | ACS Catal. 2014, 4, 2379−2386

Table 1. Characterized Data of Pd/ZnO Catalysts Summarized by CO-FTIR, TEM, and XRD

	catalysts					
	2Pd/ZnO-N	4.8Pd/ZnO-N	9.1Pd/ZnO-N	1Pd/ZnO-P	4.8Pd/ZnO-P	9.1Pd/ZnO-P
dimension perpendicular to ZnO(100), nm	20.7	20.6	23.1	>100	>100	>100
dimension perpendicular to ZnO (002), nm	39.6	34.2	42.6	>100	>100	>100
dimension perpendicular to ZnO (101), nm	22.3	20.6	23.6	>100	>100	>100
Pd_xZn_y average size using TEM, nm	2	3	4.7	2	5.5	8.3
PdZn size using XRD, nm		4	16		28	32
dominant Pd_xZn_y phase	Pd-rich PdZn	Pd-rich PdZn	Pd-rich PdZn and $PdZn_\beta$	Pd-rich PdZn	$PdZn_\beta$	$PdZn_\beta$

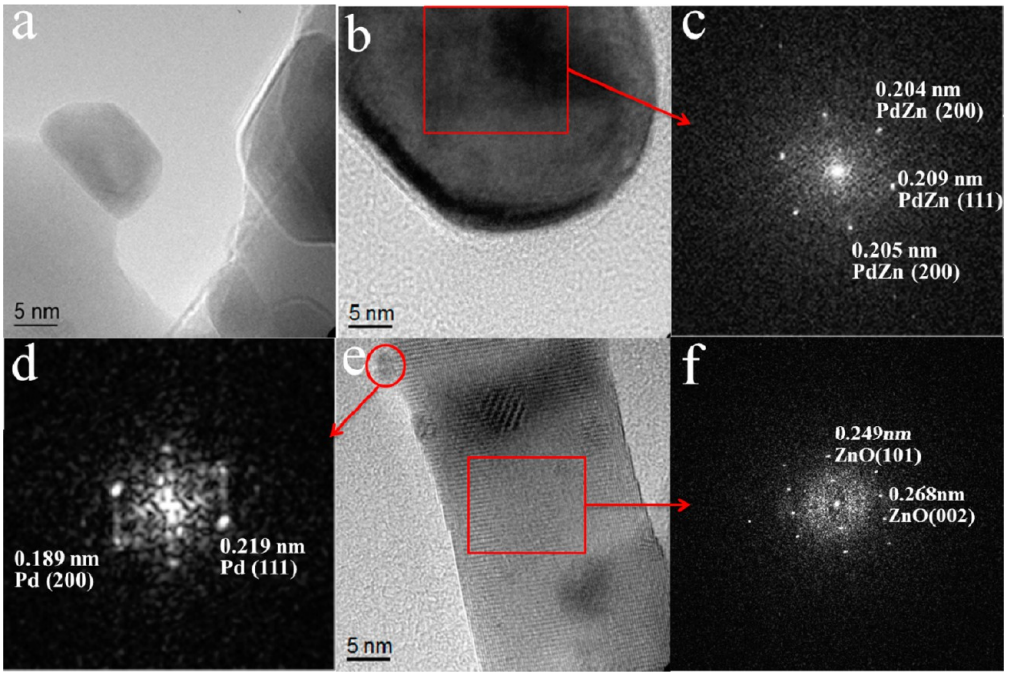

Figure 5. HR-TEM images and area-indexed images of Fourier transforms of 9.1 Pd/ZnO-N.

3.3. Surface Composition (Pd_xZn_y Phase) of Pd/ZnO Catalysts. To further explorer the active phase of the Pd/ZnO catalysts, HRTEM was used to identify the structure of the PdZn particles. Figure 5 shows HRTEM images of the 9.1%Pd on ZnO needles. Both $PdZn_\beta$ alloy phase (Figure 5a–c) and Pd-like phases, like either fcc metallic Pd or a solid solution of Zn in fcc Pd, a so-called $PdZn_\alpha$ phase (Figure 5d, e), were observed on the samples. Figure 5f further confirms that the predominantly exposed ZnO facet is (10-10) nonpolar planes.

Our previous work showed that in situ CO-FTIR can be used to distinguish the surface PdZn alloy and metallic Pd. When $Pd/ZnO/Al_2O_3$ catalyst was reduced at low temperatures where metallic Pd was present, both linear adsorption at 2065 $cm^{-1}$and bridge adsorption at 1985 cm^{-1} were detected. When $Pd/ZnO/Al_2O_3$ catalyst was reduced at high temperatures and PdZn alloy was formed, only one CO linear adsorption peak at 2076 cm^{-1} was observed.[36] Herein, to understand the surface composites of catalysts, CO-FTIR experiments were operated on the Pd/ZnO catalysts (Figure 6). The CO-FTIR spectra of different CO pressures on 2% Pd/ZnO-N show that a main band at 2041 cm^{-1} was observed at low CO pressure (i.e., 0.024 Torr, Figure 6a), which is close to the one with CO linear adsorption on metallic Pd.[35] It is well-known that a bridging CO adsorption peak would appear first, and both linear and bridged CO adsorption would be present on metallic Pd with the increase of CO pressures.[37]

Our other CO pressures experiments (Figure 6a) reveal only one linear CO absorption peak, although it slightly red-shifts to 2049 cm^{-1}. It suggests that the peak at 2041 cm^{-1} could not be simply assigned to the CO linear adsorption on metallic Pd, but instead, could be assigned to our proposed Pd_xZn_y ($x > y$). Similarly, the CO-FTIR spectra of different CO pressures on 4.8% Pd/ZnO-N also show one main band at 2062 cm^{-1} (Figure 6b), which shifts to 2067 cm^{-1} with increasing CO pressure. At even higher Pd loading (i.e.,9.1% Pd/ZnO-N), with the increase of CO pressure, a linear CO adsorption band at 2072 cm^{-1} was first observed and further red-shifted to 2078 cm^{-1} (Figure 6c), which is characteristic CO adsorption on $PdZn_\beta$ phase.[35] Notably, another two bands with peaks at 1972 and 1862 cm^{-1} appeared, and the intensity further increased at CO pressures above 0.07 Torr. The two bands were assigned to the CO adsorption on either metallic Pd[35,36] or Pd-rich Pd_xZn_y,[38] which could be developed after CO adsorption,[39] or during the H_2 pretreatment of the catalysts.

Figure 6d further compares the CO-FTIR spectra of Pd/ZnO-N with different Pd loadings after the surface of catalysts was fully saturated with CO. It is clear that, as the Pd loading increases, the intensity of linear CO decreases significantly. This suggests a decreased dispersion of Pd_xZn_y alloy particles, consistent with the XRD and TEM results. In the meantime, the peak shifted to high wavenumbers monotonically. The changes in the CO band with Pd loadings on the nonpolar (10-

dx.doi.org/10.1021/cs500590t | ACS Catal. 2014, 4, 2379–2386

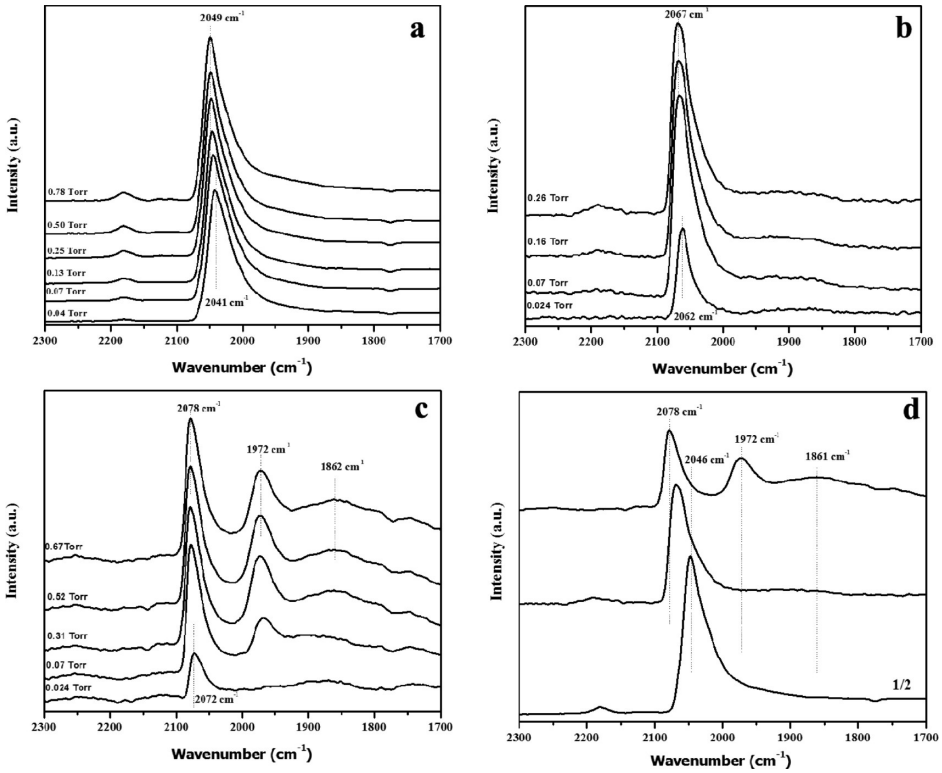

Figure 6. CO-FTIR spectra of different CO pressures on (a) 2 wt % Pd/ZnO-N, (b) 4.8 wt % Pd/ZnO-N, (c) 9.1 wt % Pd/ZnO-N, and (d) CO-FTIR spectra Pd/ZnO-N with different Pd loading with saturated CO. All the samples, before CO adsorption, were reduced in situ at 400 °C for 2 h.

10) facets suggest either the formation of Pd_xZn_y alloys of different compositions or interactions between CO and Pd_xZn_y, which varies with particle size. However, the latter may be less likely based on the discussions below by comparing the CO-FTIR of Pd_xZn_y alloy with the same particle size over different ZnO facets. The red shift of the linear CO band with Pd loading is thus correlated to the formation of different structural Pd_xZn_y alloys on the nonpolar (10-10) facet of ZnO. At low Pd loadings (i.e., 2 wt % Pd), Pd_xZn_y with $x > y$ are formed. Upon increasing the Pd loading, the ratio of x/y decreases correspondingly. With higher Pd loadings (e.g., 9.1 wt % Pd/ZnO-N), although the $PdZn_\beta$ phase ($x/y = 1$) was formed on the nonpolar (10-10) surface, other Pd-rich Pd_xZn_y phases were also observed in CO-FTIR. It is still unclear why different Pd_xZn_y alloy phases are formed as a function of Pd loading on the ZnO-N; however, it will not affect our conclusion that the formation of pure and stable $PdZn_\beta$ seems to be hindered on the nonpolar (10-10) facets.

For Pd/ZnO-P catalysts (Supporting Information Figure S4 and S5), only one main band at 2058−2068 cm^{-1} was observed, depending on the CO coverage on 1% Pd/ZnO-P, which can be attributed to linear adsorbed CO over the Pd_xZn_y alloy. It is important to note that despite the similar particle sizes of the Pd_xZn_y alloy on 1 wt %Pd/ZnO-P and 2Pd/ZnO-N (i.e., ∼2 nm), the bands of linearly adsorbed CO are significantly different (2058 vs 2041 cm^{-1}), indicating the different structures of the Pd_xZn_y alloy on the two supports (i.e., different x/y ratios). Given the similar chemical shifts, however, the structure of the Pd_xZn_y alloy on 1%Pd/ZnO-P should be similar to that of 4.8 wt % Pd/ZnO-N, evidenced by the single peak at ∼2062 cm^{-1} in both cases. This suggests that, instead of particle size, in our studies, the composition of the Pd_xZn_y alloy is more related to the chemical shift of the linear CO band. At higher Pd loading (i.e., 4.8 wt % Pd/ZnO-P), a main band at 2075 cm^{-1} with a small hump at 1920 cm^{-1} was observed, suggesting the predominant formation of $PdZn_\beta$ phase.[8] The small hump at 1920 cm^{-1} is attributed to the bridging CO on metallic Pd, likely due to the incomplete transformation of metallic Pd to $PdZn_\beta$ alloy by the lower pretreatment temperature (i.e., 300 °C). Interestingly, different from those on the 9.1% Pd/ZnO-N (Figure 6d), no other peaks were developed, and the hump at 1920 cm^{-1} also showed no clear changes with the increased CO coverage on the 4.8 wt % Pd/ZnO-P, suggesting the formation of a pure and stable $PdZn_\beta$ phase on ZnO-P with nondominant facets. On 9.1 wt % Pd/ZnO-P, CO-FTIR could not detect obvious signal of CO adsorption. This is mainly due to the poor PdZn dispersion, as confirmed by our TEM observations.

CO oxidation experiments were also used to identify the PdZn phase for Pd/ZnO catalysts with low Pd loading amounts.[40] It was identified that 1% Pd/ZnO-P, 2% Pd/ZnO-N, and 4.8% Pd/ZnO-N are not composed of $PdZn_\beta$, but instead, have the Pd-rich PdZn phase (e.g., $PdZn_\alpha$), based on the comparison between total number of active sites using different standard catalysts (pure Pd, $PdZn_\alpha$, $PdZn_\beta$) and the total number of Pd atoms in Pd/ZnO catalysts, which is consistent with the results by CO-FTIR (Supporting Information Tables S1 and S2).

3.4. CO Selectivity of Pd/ZnO Catalysts in MSR. Considering the fact that ZnO-N and ZnO-P supports have different surface areas and, consequently, different metal dispersions at a similar Pd loading, Figure7 compares the CO selectivity as a function of Pd loading amount for both ZnO-N- and ZnO-P-supported Pd catalysts at similar methanol conversion. Separate experiments on pure ZnO-N and ZnO-P show a very low reactivity for MSR, with methanol conversions

dx.doi.org/10.1021/cs500590t | ACS Catal. 2014, 4, 2379−2386

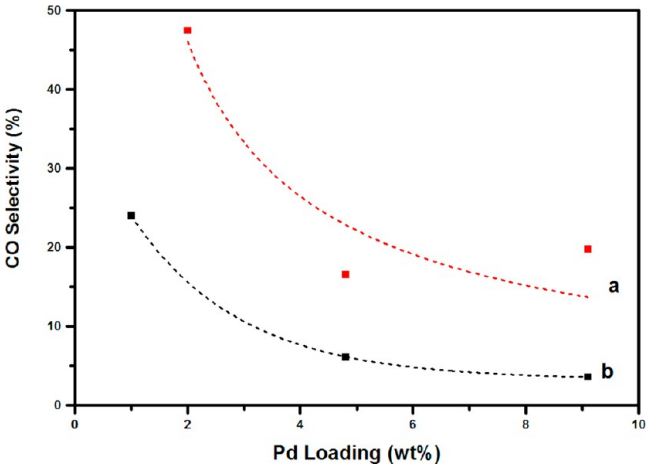

Figure 7. CO selectivity of Pd/ZnO-N (a) and Pd/ZnO-P (b) with Pd loading amount under methanol conversion of 30−40%. 100−200 mg catalyst, $P_{methanol}$ = 6.4 mol %, W/F = 0.037−0.123 g·s·mL^{-1}, T = 250 °C.

being ∼3% of that of corresponding Pd/ZnO catalysts under the same reaction conditions, confirming the negligible activity from the supports. From Figure 7, we can see that CO selectivity decreases with an increase in the Pd loading for both Pd/ZnO-P and Pd/ZnO-N catalysts. This is not surprising because a higher Pd loading typically results in a larger particle size of PdZn, which is known to exhibit a lower CO selectivity in MSR.[6] In addition, Pd/ZnO-N catalysts exhibit higher CO selectivity than Pd/ZnO-P catalysts at the same Pd loading. More importantly, even compared at a similar particle size of PdZn, the CO selectivity of Pd/ZnO-N is higher than that of Pd/ZnO-P (e.g., 2 wt % Pd/ZnO-N versus 1 wt % Pd/ZnO-P with ∼2 nm Pd_xZn_y particle size; 9.1 wt % Pd/ZnO-N versus 4.8 wt % Pd/ZnO-P with ∼5 nm Pd_xZn_y particle size, shown in Table 1 and Figure 7).

Figure 8 further compares CO selectivity as a function of methanol conversion over 2 wt % Pd/ZnO-N and 1 wt % Pd/ZnO-P catalysts with a similar Pd_xZn_y particle size (∼2 nm). Both catalysts show a similar trend in terms of CO selectivity

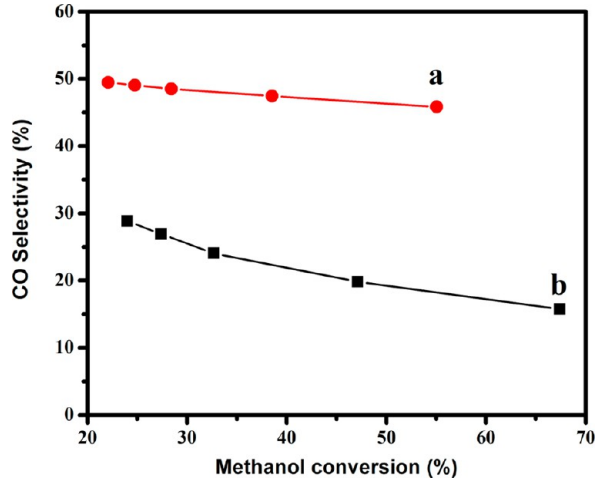

Figure 8. CO selectivity as a function of methanol conversion of the MSR reaction over the dominant Pd-rich PdZn phase catalysts: (a) 2% Pd/ZnO-N; (b) 1% Pd/ZnO-P. 100−200 mg catalyst, $P_{methanol}$ = 6.4 mol %, W/F = 0.037−0.493 g·s·mL^{-1}, T = 250 °C.

versus methanol conversion; namely, CO selectivity decreases with increasing methanol conversion, likely as a result of the limited CO oxidation. More importantly, in the range of methanol conversion studied, CO selectivity on Pd/ZnO-N is much higher than that of Pd/ZnO-P catalysts at the same methanol conversion, indicating the ZnO facet also indeed plays pivotal roles in the reaction pathway of MSR. In addition, the methanol TOF of 1 wt % Pd/ZnO-P is slightly higher than that of 2 wt % Pd/ZnO-N (Supporting Information Table S1), which matches well with the studies of model catalysts.[20]

Our previous studies on the ZnO (1010) and ZnO (0001) single crystal indicated that PdZn alloy formation is facile on the ZnO (0001) polar facets.[20] Herein, our powder catalysts with tailored facets further confirmed that it is, indeed, more difficult to form the pure and stable $PdZn_\beta$ alloy on the nonpolar (10-10) ones of ZnO-N. Instead, the polar (0001) facets play a key role in the facile formation of the pure and stable $PdZn_\beta$ phase on ZnO-P support. Over ZnO-N support with dominant nonpolar (10-10) facets, CO-FTIR, CO oxidation reaction and HRTEM unambiguously proved that Pd_xZn_y alloys ($x > y$) are dominant at low Pd loading (i.e., 2 and 4.8 wt % Pd) and gradually transformed to $PdZn_\beta$ phases (Pd_xZn_y, $x = y$) via decreasing the x/y ratios as Pd loading increases. On 9.1 wt % Pd/ZnO-N, although $PdZn_\beta$ phases are formed, other Pd-rich Pd_xZn_y and even segregated Pd coexisted or they possibly were developed after CO adsorption. The Pd-rich Pd_xZn_y phases ($x > y$) have been reported to be responsible for the high CO selectivity in MSR.[14,15] Consistent with the recent report,[14] high CO selectivity has been observed on the Pd/ZnO-N catalysts as a result of the predominant formation of the Pd-rich phase of different compositions.

On the ZnO-P support without dominant facets, the Pd-rich Pd_xZn_y ($x > y$) phase was also observed at very low Pd loadings (e.g., 1 wt % Pd). It is interesting to find out that the structures of the Pd_xZn_y alloy on 1 wt % Pd/ZnO-P are similar to that on 4.8 wt % Pd/ZnO-N, which is confirmed by the similar linear CO adsorption at ∼2065 cm^{-1} (Figure 6b, Supporting Information Figure S6). Most importantly, the two samples showed comparable CO selectivity at similar methanol conversions, further confirming the similar Pd_xZn_y structure on the two catalysts. In addition, it also indicates that Pd might preferentially deposit onto the nonpolar (10-10) facet of ZnO-P at low Pd loading.

As the Pd loading increases, Pd deposits onto the polar (0001) facets to form the pure and stable $PdZn_\beta$ on ZnO-P supports. A higher Pd loading (i.e., 4.8 wt % Pd/ZnO-P) is thus required to form the stable $PdZn_\beta$ phase that facilitates the CO_2 formation and thus decreases CO selectivity on the Pd/ZnO-P catalysts. In addition, the particle size of PdZn alloy has been previously reported to be correlated to the CO selectivity in MSR.[6−8] The smaller the particle size, the higher the CO selectivity.[6] For example, a low Pd loading amount (e.g., 0.5 wt % Pd) was found to result in smaller PdZn nanoparticles and thus a high CO selectivity in MSR on commercial ZnO-supported Pd catalysts.[6] Our current results further reveal that, in addition to the particle size, the higher CO selectivity at lower Pd loading could also be due to the formation of Pd-rich Pd_xZn_y preferentially on ZnO nonpolar facets. Such insight can be used to guide the design of more selective PdZn catalysts for MSR.

dx.doi.org/10.1021/cs500590t | ACS Catal. 2014, 4, 2379−2386

4. CONCLUSION

Two stable supports of ZnO-N and ZnO-P with different fractions of nonpolar facets have been used to study the effects of ZnO facet on the formation of PdZn alloys and their catalytic performances in MSR. Our results reveal that, depending on the Pd loading, Pd_xZn_y phases of various compositions are formed on the nonpolar (10-10) facets of ZnO. At low Pd loadings (<4.8 wt %), Pd-rich phases (Pd_xZn_y, $x > y$) are predominant, and the x/y ratio decreases with an increase in Pd loading, leading to the decreased CO selectivity on the Pd/ZnO-N catalysts. At high Pd loadings (e.g., 9.1 wt % Pd/ZnO-N), although $PdZn_\beta$ phase can be formed, other Pd-rich Pd_xZn_y and even segregated Pd coexist, leading to high CO selectivity. On the other hand, formation of stable $PdZn_\beta$ was found to be facile on polar (0001) facets, which results in low CO selectivity. It is also proposed that on a ZnO support without dominant facet (e.g., ZnO-P), Pd first selectively deposits onto the nonpolar (10-10) facets to form Pd-rich Pd_xZn_y ($x > y$) phases, resulting with high CO selectivity, such as the case with 1 wt % Pd/ZnO-P. Therefore, a higher Pd loading is required to achieve a stable $PdZn_\beta$ phase as well as high CO_2 selectivity on the Pd/ZnO-P catalysts (e.g., 4.8 wt % Pd/ZnO-P).

■ ASSOCIATED CONTENT

Supporting Information

Further details are given in Figures S1−S6 and Tables S1 and S2. This material is available free of charge via the Internet at http://pubs.acs.org.

■ AUTHOR INFORMATION

Corresponding Author

*E-mail: yong.wang@pnnl.gov.

Notes

The authors declare no competing financial interest.

■ ACKNOWLEDGMENTS

We greatly acknowledge financial support by the U.S. Department of Energy (Grant No. DE-FG02-05ER15712). We thank Andrew DeLaRiva (University of New Mexico) for doing the CO oxidation reactivity measurements. He Zhang thanks Dr. Feng Gao (PNNL) for the helpful discusson about the CO-FTIR results.

■ REFERENCES

(1) Amphlett, J. C.; Creber, K. A. M.; Davis, J. M.; Mann, R. F.; Peppley, B. A.; Stokes, D. M. *Int. J. Hydrogen Energy* **1994**, *19*, 131−137.

(2) Sa, S.; Silva, H.; Brandao, L.; Sousa, J. M.; Mendes, A. *Appl. Catal., B* **2010**, *99*, 43−57.

(3) Wei, Z. H.; Sun, J. M.; Li, Y.; Datye, A. K.; Wang, Y. *Chem. Soc. Rev.* **2012**, *41*, 7994−8008.

(4) Davidson, S. D.; Zhang, H.; Sun, J.; Wang, Y. *Dalton Trans.* **2014**, DOI: 10.1039/c1034dt00521j.

(5) Iwasa, N.; Masuda, S.; Ogawa, N.; Takezawa, N. *Appl. Catal., A* **1995**, *125*, 145−157.

(6) Dagle, R. A.; Chin, Y.-H.; Wang, Y. *Top. Catal.* **2007**, *46*, 358−362.

(7) Karim, A. M.; Conant, T.; Datye, A. K. *Phys. Chem. Chem. Phys.* **2008**, *10*, 5584−5590.

(8) Karim, A.; Conant, T.; Datye, A. *J. Catal.* **2006**, *243*, 420−427.

(9) Iwasa, N.; Mayanagi, T.; Nomura, W.; Arai, M.; Takezawa, N. *Appl. Catal., A* **2003**, *248*, 153−160.

(10) Matsumura, Y. *Appl. Catal., A* **2013**, *468*, 350−358.

(11) Xia, G.; Holladay, J. D.; Dagle, R. A.; Jones, E. O.; Wang, Y. *Chem. Eng. Technol.* **2005**, *28*, 515−519.

(12) Halevi, B.; Peterson, E. J.; DeLaRiva, A.; Jeroro, E.; Lebarbier, V. M.; Wang, Y.; Vohs, J. M.; Kiefer, B.; Kunkes, E.; Havecker, M.; Behrens, M.; Sehloegl, R.; Datye, A. K. *J. Phys. Chem. C* **2010**, *114*, 17181−17190.

(13) Peterson, E. J.; Halevi, B.; Kiefer, B.; Spilde, M. N.; Datye, A. K.; Peterson, J.; Daemen, L.; Llobet, A.; Nakotte, H. *J. Alloys Compd.* **2011**, *509*, 1463−1470.

(14) Halevi, B.; Peterson, E. J.; Roy, A.; DeLariva, A.; Jeroro, E.; Gao, F.; Wang, Y.; Vohs, J. M.; Kiefer, B.; Kunkes, E.; Havecker, M.; Behrens, M.; Schlogl, R.; Datye, A. K. *J. Catal.* **2012**, *291*, 44−54.

(15) Friedrich, M.; Teschner, D.; Knop-Gericke, A.; Armbruster, M. *J. Catal.* **2012**, *285*, 41−47.

(16) Friedrich, M.; Penner, S.; Heggen, M.; Armbruster, M. *Angew. Chem., Int. Ed.* **2013**, *52*, 4389−4392.

(17) Saito, M.; Wagner, T.; Richter, G.; Ruehle, M. *Phys. Rev. B* **2009**, *80*, 134110.

(18) McLaren, A.; Valdes-Solis, T.; Li, G.; Tsang, S. C. *J. Am. Chem. Soc.* **2009**, *131*, 12540−12541.

(19) Halevi, B.; Lin, S.; Roy, A.; Zhang, H.; Jeroro, E.; Vohs, J.; Wang, Y.; Guo, H.; Datye, A. K. *J. Phys. Chem. C* **2013**, *117*, 6493−6503.

(20) Hyman, M. P.; Lebarbier, V. M.; Wang, Y.; Datye, A. K.; Vohs, J. A. *J. Phys. Chem. C* **2009**, *113*, 7251−7259.

(21) Ertl, G. *Catal. Rev.: Sci. Eng.* **1980**, *21*, 201−223.

(22) Spencer, N. D.; Schoonmaker, R. C.; Somorjai, G. A. *J. Catal.* **1982**, *74*, 129−135.

(23) Martono, E.; Hyman, M. P.; Vohs, J. M. *Phys. Chem. Chem. Phys.* **2011**, *13*, 9880−9886.

(24) Kwak, G.; Yong, K. J. *J. Phys. Chem. C* **2008**, *112*, 3036−3041.

(25) Tian, N.; Zhou, Z.-Y.; Sun, S.-G.; Ding, Y.; Wang, Z. L. *Science* **2007**, *316*, 732−735.

(26) Xu, R.; Wang, D.; Zhang, J.; Li, Y. *Chem.—Asian J.* **2006**, *1*, 888−893.

(27) Xie, X.; Li, Y.; Liu, Z.-Q.; Haruta, M.; Shen, W. *Nature* **2009**, *458*, 746−749.

(28) Li, G. R.; Hu, T.; Pan, G. L.; Yan, T. Y.; Gao, X. P.; Zhu, H. Y. *J. Phys. Chem. C* **2008**, *112*, 11859−11864.

(29) Wu, Z. L.; Li, M. J.; Overbury, S. H. *ChemCatChem.* **2012**, *4*, 1653−1661.

(30) Andelman, T.; Gong, Y. Y.; Polking, M.; Yin, M.; Kuskovsky, I.; Neumark, G.; O'Brien, S. *J. Phys. Chem. B* **2005**, *109*, 14314−14318.

(31) Burton, P. D.; Peterson, E. J.; Boyle, T. J.; Datye, A. K. *Catal. Lett.* **2010**, *139*, 26−32.

(32) Zhang, J.; Liu, H.; Wang, Z.; Ming, N.; Li, Z.; Biris, A. S. *Adv. Funct. Mater.* **2007**, *17*, 3897−3905.

(33) Sun, J. M.; Ma, D.; Zhang, H.; Liu, X. M.; Han, X. W.; Bao, X. H.; Weinberg, G.; Pfander, N.; Su, D. S. *J. Am. Chem. Soc.* **2006**, *128*, 15756−15764.

(34) Wang, C. L.; Shen, E. H.; Wang, E. B.; Gao, L.; Kang, Z. K.; Tian, C. G.; Lan, Y.; Zhang, C. *Mater. Lett.* **2005**, *59*, 2867−2871.

(35) Conant, T.; Karim, A. M.; Lebarbier, V.; Wang, Y.; Girgsdies, F.; Schloegl, R.; Datye, A. *J. Catal.* **2008**, *257*, 64−70.

(36) Lebarbier, V.; Dagle, R.; Conant, T.; Vohs, J. M.; Datye, A. K.; Wang, Y. *Catal. Lett.* **2008**, *122*, 223−227.

(37) Szanyi, J.; Kuhn, W. K.; Goodman, D. W. *J. Vac. Sci. Technol., A* **1993**, *11*, 1969−1974.

(38) Bronstein, L. M.; Chernyshov, D. M.; Volkov, I. O.; Ezernitskaya, M. G.; Valetsky, P. M.; Matveeva, V. G.; Sulman, E. M. *J. Catal.* **2000**, *196*, 302−314.

(39) Gao, F.; Wang, Y. L.; Goodman, D. W. *J. Phys. Chem. C* **2009**, *113*, 14993−15000.

(40) Johnson, R. S.; DeLaRiva, A.; Ashbacher, V.; Halevi, B.; Villanueva, C. J.; Smith, G. K.; Lin, S.; Datye, A. K.; Guo, H. *Phys. Chem. Chem. Phys.* **2013**, *15*, 7768−7776.